Transition Dynamics of Frictional Granular Clusters

Antoinette Tordesillas [*], David M. Walker [*], Gary Froyland [†], Jie Zhang [‡], Robert P. Behringer [‡]

[*]Department of Mathematics and Statistics, University of Melbourne, Parkville, VIC 3052 Australia,[†]School of Mathematics and Statistics, University of New South Wales, Sydney NSW 2052 Australia, and [‡]Department of Physics, Duke University, Durham, NC 27708 USA

Force chains, the primary load-bearing structures in dense granular materials, rearrange in response to applied stresses and strains. These self-organized grain columns rely on contacts from weakly stressed grains for lateral support to maintain and find new stable states. But, the regulation of the topology of contacts and strong-versus-weak forces through such contacts remains unclear. This study of local self-organization of frictional particles in a deforming dense granular material exploits a transition matrix to quantify preferred conformations and the most likely conformational transitions. It reveals favored cluster conformations reside in distinct stability states, reminiscent of "magic numbers" for molecular clusters. To support axial loads, force chains typically reside in more stable states of the stability landscape, preferring stabilizing truss-like, 3-cycle contact topologies with neighboring grains. The most likely conformational transitions during force chain failure by buckling correspond to rearrangements among, or loss of, contacts which break the 3-cycles.

force chains | Markov transition dynamics | clusters | stability

Granular materials (e.g. soil, mineral ores, powders, cereals grains), an ubiquitous form of matter, are at the heart of many important natural phenomena and man-made processes. While these materials have stimulated intense research activity for decades [1, 2, 3, 4], robust predictions of their mechanical behavior under load remain elusive [5, 6, 7, 8, 9, 10]. In particular, the quasi-static deformation and flow of dense granular materials exhibit hallmarks of complexity including self-organization [11, 12, 13, 14, 15, 17, 16, 18] and cooperative evolution among emergent mesoscopic structures [19, 20, 21]. Precise knowledge of the rules for self-organization is crucial for reliable model predictions used to: forecast and mitigate natural disasters (e.g. earthquakes, landslides) [24, 25, 26]; improve road and off-road transport infrastructure [27]; and develop measures which meet the unprecedented demands for mineral resources amid supply and energy constraints [28, 3, 4], to highlight a few examples. The mechanical response of a granular material to applied forces is governed by the rearrangements of constituent particles whose vast collective degrees of freedom lead to emergent complexity [29, 30, 31, 32]. To date, the crucial missing element that limits prediction and control of granular behavior, particularly its failure, is quantitative understanding of the interplay between dynamical particle rearrangements, and the evolution of key functional structures, epitomized by major load-bearing force chains (Supplementary Fig. 1, Supplementary Movie 1) [10, 33, 35, 36, 37, 30, 38].

Recent numerical and experimental developments in the physics and mechanics of dense granular media have yielded insights into how structural behavior at the scale of a few grains leads to failure at the macroscopic scale [12, 13, 17, 18, 15, 14, 19, 20, 21, 39, 26, 16, 30, 22]. By failure, we mean that a macroscopic sample of material loses its ability to resist an applied shear stress or strain. The formation of shear bands has been implicated as a key element in such mechanical failure. A shear band is a region in the material in which deformation and particle rotations are concentrated. Once fully developed, shear bands split

the granular body into parts which then move relative to each other in near-rigid body motion (Supplementary Movie 2) [11, 40, 39, 41, 17]. On a large scale, this is exemplified in the relative movement of opposing rock faces along an earthquake fault [24, 26]. Grain-scale information from noninvasive micromechanical experiments on sand and photoelastic disk assemblies suggests that force chains fail by buckling, and that their collective localized buckling is the mechanism underpinning shear band formation and, ultimately, macroscopic failure [11, 13]. A comprehensive experimental and numerical investigation into force chain buckling in a series of monotonic and cyclic shear tests, for a range of granular materials corroborate this [38, 15, 14, 16, 20, 19, 31, 21]. Moreover, cooperative evolution among linear and cyclic building blocks of self-organization, i.e. force chains and surrounding minimal contact cycles, has been observed [20, 19, 21, 22]. So far, however, how force chains regulate their contacts with respect to both topology and the forces they carry for a given loading condition is largely unknown (Supplementary Fig. 1). An overarching question is whether particles rearrange in response to the changing applied forces to provide optimum stability to these axially loaded columns of grains (Supplementary Movie 1). Transition pathways between granular cluster conformations in a stability landscape would provide such information, but to date, these have not been established for *any* granular system. Here we report on the first study of these transition pathways from the standpoint of cluster topology and structural stability. By probing relative probabilities of cluster conformations and conformational transitions we find that there are favored conformations residing in distinct structural stability states. Analysis of stability transitions and associated dynamical barriers elucidate the role of topology in the stability and failure by buckling of force chains.

Mesoscale conformations and conformational transitions of granular self-organization. Here, we examine a bidisperse, densely-packed assembly of frictional circular disks subject to quasi-static cyclic shear under constant volume: see Methods and Fig. 1 *top left* for an image of the assembly with the stresses visualized from birefringence patterns in the photoelastic disks (Supplementary Movie 1). The positions of the particles and their contacts, contact forces, displacements and rotations are measured in each state. A shear band develops at some stages of each shear cycle (Supplementary Movie

---

Reserved for Publication Footnotes

2). The evolving mechanical response of the granular material is characterized by analysis of the individual equilibrium states, each corresponding to a strain state in the loading history, and their sequential state-to-state transitions. For each equilibrium state, an unweighted and undirected mathematical graph models the particles as the nodes, and their contacts as the connecting links or edges between corresponding nodes [42, 19, 21]. Particle rearrangements are primarily responsible for the material's deformation. These are reflected in the evolving complex network of contacts: old network connections break as contacts are lost, while new connections form as contacts are created (Supplementary Movie 1). In this study, we focus on that class of mesoscopic cluster conformations comprising a particle and its first ring of contacting neighbors (analogous to the first coordination shell in molecular clusters). This class comprises the smallest clusters for which emergent preferential orientations in contacts and contact forces can be comprehensively probed. Next we sort the clusters according to the network properties of degree (number of contacts of the central reference particle) and number of 3-cycles within the cluster [42, 19, 43]. The physical and geometrical restrictions imposed by the particle size distribution and the system boundaries imply a finite number of distinct cluster conformations involving one node (particle) and its connected neighbors. We found 28 distinct cluster conformations after examining the first ring of contacting neighbors of each particle at every state throughout loading. Fig. 1 *top right* shows the subgraphs of the conformations, each labelled x_j^i: x is the central particle degree, i is the number of 3-cycles, j is the number of shared edges among these 3-cycles.

The transitions between the 28 cluster conformations are modeled as a discrete time Markov process [44] with one time step representing an interval of four quasi-static equilibrium states, i.e. the number of times a particle of a given conformation transforms to another conformation, possibly of the same topology, after four time steps (see, Methods for an explanation on how to select a suitable time step interval). The corresponding 28×28 transition matrix is analyzed to extract the most prevalent conformations and to identify sets of conformations which are almost-invariant under the dynamics, i.e. the most persistent sets of conformations [44]. In order of decreasing frequency, the most recurrent granular conformations are 3_0^0, 2_0^0, 4_0^0, 4_0^1 and 3_0^1 (Fig. 1 *bottom left*). Almost-invariant transition sets of granular conformations are identified from the eigenvectors of the transition matrices. The number of sets are determined by the separation of the spectrum of eigenvalues using a clustering algorithm [44]; Fig. 1 *bottom left* shows four almost-invariant sets found using three eigenvectors. Conformations of similar degree typically lie in the same set, with the distinction between members of each set being mainly due to the rearrangements of the first ring neighbors (i.e. no loss or gain of contacts): see Fig. 1 *bottom right*. The top five conditional transition probabilities $p(x_j^i \rightarrow y_l^k)$, quantifying conformational transitions from x_j^i to y_l^k are: $p(2_0^0 \rightarrow 2_0^0) = 0.1771$, $p(3_0^0 \rightarrow 3_0^0) = 0.1696$, $p(2_0^0 \rightarrow 3_0^0) = 0.0708$, $p(3_0^0 \rightarrow 2_0^0) = 0.0689$, $p(4_0^0 \rightarrow 4_0^0) = 0.0589$.

Topology and dynamics of force chains. The strength of a granular assembly under load, i.e. its resistance to particle rearrangements or deformation, comes from two sources. One is inherent (e.g. initial packing, particle shape and surface properties); the other is induced by the loading conditions, i.e. by self-organization. Recent evidence of cooperative behavior among emergent mesoscopic structures, such as the formation of truss-like 3-cycles around force chains, provides

incisive clues for functional activity with governing design principles resembling those employed in architectural structures [20, 21, 19, 22].

Force chains are prone to fail by buckling [33, 11, 34, 38, 15]. To function effectively, these primary axial load-bearing columns of grains must be supported laterally through contacts with comparatively weak neighboring particles [38]. Past studies have revealed strong similarities in force chain behavior for a wide range of material properties and boundary conditions [38, 14, 16, 20, 21]. Here we find that, at any given equilibrium state, force chain particles make up from 10% to 60% of the total number of particles corresponding to unjammed and jammed states, respectively [16, 20]. We find these force chains reside in regions of relatively high connectivity, as evident in their higher average degree and clustering coefficient (a measure of the density of 3-cycle configurations in a network [21, 22]).

As in past studies, we find that force chains favor contacts with laterally supporting neighbors in 3-cycle, truss-like formations [19, 20], specifically, through conformation 4_0^1 (Fig. 2, Supplementary Figs. 1 & 2). Non-force chains frequently, though not exclusively comprise particles in less connected conformations 2_0^0 and 3_0^0, which have no 3-cycles. A dual buckling resistance underpins this cooperative evolution between columnar force chains and truss-like 3-cycles: 3-cycles i) 'prop-up' the force chain to restore alignment (Fig. 2, Supplementary Figs. 1 & 2), and ii) frustrate particle rotations integral to buckling [19, 22].

Force chains are not only primary load bearers, but are also major repositories of stored energy in the system [23, 37, 14, 33]. Consequently, their failure by buckling directly: i) reduces the load the material can carry, and ii) leads to dissipation following the collective release of stored energy accumulated at member contacts [14, 15, 38]. For instance, note the decrease in the brightness of the birefringence pattern in Fig. 2 (Supplementary Fig. 1) as a force chain buckles. Load-carrying capacity and energy dissipation form the two halves of mathematical formulations that relate the deformation to the stress in a dissipative material (i.e. continuum models). To achieve reliable and robust predictions, such models must incorporate the kinematics of those rearrangement events which are chiefly responsible for energy dissipation (i.e. internal variables or plastic strains [6, 10, 29, 31]). Knowing what conformational transitions are likely to occur when a force chain buckles and their associated probabilities, forms an essential and heretofore missing element in continuum models [10, 38]. To date, the modeler's only recourse has been to offer either an "educated guess' [10, 38] or empirical evolution laws for the plastic strain with no clear connection to the geometric or mechanical details associated with force chain buckling [37, 5, 29]. This study shows that, within a buckling force chain, the most likely conformational transitions tend to either preserve the topology or involve a transition from a more connected conformation (i.e. 3_0^1 or 4_0^1) to a less connected conformation (i.e. 3_0^0), as seen in Fig. 2 and Supplementary Figs. 1 & 2. Conformational transitions from 4_0^1 to 3_0^0 involve loss of both a contact and supporting 3-cycle. Such transitions are not the most dominant within the assembly, indicating that buckling does not have to be rife to induce formation of shear bands and/or global failure. This confirms past findings on the initiation of failure in dense systems from numerical and experimental data [15, 14, 38, 20, 31].

Conformational stability, transitions and dynamical barriers. With the recently developed techniques from structural mechanics [20] and the ability to measure contact forces [12, 16, 45], we can now compute the structural stability of the clus-

ter conformation for each particle, at every equilibrium state of the loading history – and study their transition dynamics. The structural stability measure in Tordesillas et al. [20] depends on material properties, the contact forces, as well as the number, positions and directions of contacts within the cluster. From the frequency distribution of conformational stabilities, we find pronounced peaks that persist throughout the loading history (Fig. 3). That such persistent peaks emerge in the stability landscape is surprising, given the extreme heterogeneity in the factors that govern the evolution of stability of a particle relative to its first ring of contacting neighbors. The most dominant conformations and conformational transition sets (sets $1 - 4$ in Fig. 1 *bottom*) mainly lie within the stability peaks evident from the well-resolved "bands" in Fig. 3. In particular, the conformations distinguish themselves by increasing stability, which correlates well with an increasing central particle degree: for example, conformations 3_0^0 and 3_0^1 mainly reside in a lower stability peak compared to 4_0^0 and 4_0^1. The peaks in the conformational frequency distribution and the stability landscape are reminiscent of so-called "magic numbers" encountered in molecular clusters, whose physical rearrangements also govern function through ways in which topology and stability are strongly interrelated [46, 47, 48].

We next consider transition dynamics within the stability landscape (Fig. 3). Instead of directly describing transitions between the 28 conformations as a Markov chain, we partition the range of stability values (i.e. $(0, 0.1190)$) into ~ 500 contiguous intervals and model transitions between stability intervals as a Markov chain. To better resolve highly frequented stability values, we use an adaptive partition: that is, the frequency of a conformation possessing a stability value in each interval is roughly equal. We found distinct peaks in stability, Fig. 4 *top right*, that are consistent with those in Fig. 3. In particular, we find a surprisingly smooth build-up of probability density to each stability peak followed by a precipitous drop.

Sharp changes in the entries of the second largest eigenvector of the stability value transition matrix, as in Fig. 4 *right*, delineate dynamical barriers that are infrequently traversed [44]. These sharp changes partition the stability landscape into six major bands (Fig. 4 *right*): $1 : (0, 0.0315)$, $2 : (0.0315, 0.0397)$, $3 : (0.0397, 0.0472)$, $4 : (0.0472, 0.0597)$, $5 : (0.0597, 0.0630)$ and $6 : (0.0630, 0.1190)$. Transitions within each of these six bands are much more likely than transitions between different bands. This banding structure can also be seen in the block-like structure of the full stability transition matrix (Fig. 4 *left*).

By aggregating the fine stability intervals into the six large bands, we arrive at a 6×6 transition matrix describing band-to-band transitions. 60% of stability transitions are within a band. However, we also observe that inter-band stability transitions prefer to *jump over* the intervening stability band: that is, transitions between bands 1, 3, and 5 and between bands 2, 4, and 6 are favored (cf. the interlacing of low entries in the block matrix of Fig. 4 *left* and the dotted and solid demarcation of the bands in Fig. 4 *right*). Based on this observation, we can further aggregate by setting state 1 to be the union of bands 1, 3, and 5, and state 2 to be the union of bands 2, 4, and 6, to produce a 2×2 transition matrix $B = [0.9215\ 0.0768; 0.1872\ 0.8115]$ which effectively partitions the stability space into two almost-invariant stability regions, each consisting of three interlaced stability bands. That is, transitions within state 1 (stability bands 1, 3, 5) occur with probability 0.9215 and transitions within state 2 (stability bands 2, 4, 6) occur with probability 0.8115. On average 70.9% of clusters are in state 1 and 29.1% of clusters are in state 2. The diagonal dominance of B further highlights the "jumping" between every second stability band. Some of the preferred conformations (e.g. 3_0^0) appear in more than one stability band, thereby indicating that topology does not completely overshadow all other factors that influence stability.

Conformational stability transitions during force chain failure by buckling. So far we have discussed how a force chain moves, regulates its contacts as it responds to and resists an applied force, and buckles. We now focus on the stability transitions of force chain particles during this ultimate failure state of buckling – a mechanism implicated as the precursor for shear band formation and global failure in dense materials [11, 24, 26, 13, 33]. Conformations of particles in columnar force chains typically possess higher stability (Fig. 5) and those in buckling force chains (BFC) undergo a similar process of jumping over one stability band (Fig. 5 *inset*). A relatively higher probability exists for BFC transitions from higher to lower stability states than vice versa. That some force chain particles see an increase in their stability during buckling, highlights the system's continual regulation of the topology of contacts and forces to adapt and delay imminent collapse of these load-bearing structures (Supplementary Figs. 1 & 2). This is entirely consistent with earlier findings on "3-force cycles", i.e. 3-cycles whose contacts each bear above the global average force. These were found to emerge just at the time and location in the sample in greatest need of support: the onset of force chain buckling in what ends up being the shear band [19].

Past experiments and simulations have shown that the build-up of new chains and collapse by buckling of old force chains govern granular deformation in the presence of shear bands [33, 11, 34, 12, 14, 38, 13]. The "critical state regime" of soil mechanics, in which the material flows at near-steady shear stress and global volume, is believed to occur when these two processes balance each other [13, 49, 50]. Focussing on the six stability bands, we find the following: the topology of the dominant cluster in the higher stability bands has greater or equal degree relative to the dominant cluster in the lower stability bands; different stability bands can have the same dominant cluster topology; conformations of force chain particles are among the dominant conformations within a band; the topology of buckled force chain segments within a stability band follows the dominant conformation but buckling is less likely in higher stability band conformations due to the increased lateral support (see Table 1).

Linking topology, stability, dynamics and function in granular media. In summary, the mechanical response of a granular material under load – ultimately rooted in the physical motions or rearrangements of the particles – is systematically and comprehensively quantified here by a study of conformational and stability transition dynamics. We have examined the dynamics of that class of conformations consisting of a particle and its first ring of contacting neighbors in a quasi-statically deforming granular material. Relative probabilities of the 28 conformations found, and conformational transitions, have identified the prevalent and persistent rearrangements, including those in key functional structures – the primary load-bearing force chains – which govern the strength and load-carrying capacity of the material. We found self-organization towards favored equilibrium cluster conformations which, in turn, reside within favored stability states in a stability landscape with infrequently traversed dynamical barriers. The most likely conformational transitions during force

chain failure by buckling, the mechanism believed to be responsible for global granular failure, correspond to rearrangements among, or loss of, contacts which break the stabilizing truss-like 3-cycles. We note that the patterns obtained from experimental observations reported here were also found, at least qualitatively, in a discrete element simulation of a two-dimensional polydisperse assembly under monotonic biaxial compression with constant confining pressure.

The granular cluster dynamics uncovered here provides direct structural and mechanical insights into the mechanisms that underpin the rheology of granular media. Conformational transition probabilities comprehensively quantify the relative contributions of the various rearrangements to deformation, including those directly responsible for energy dissipation and global failure of the material. This opens the door to robust and tractable predictive continuum models of granular deformation and failure. The patterns of self-organization are remarkably reminiscent of those seen in molecular clusters [46, 47]. Anomalously high density stability states, populated by clusters with specific number of contacts in the first ring of neighbors, hint at the possible existence of "magic numbers" in granular systems. In contrast to molecular systems for which the complete tracking of molecular bond formation and breakage is as yet out of reach experimentally [46], granular clusters offer a unique paradigm for studies of emergence and self-organization through conformational transition dynamics: the formation and loss of contacts, as well as the force between constituent particles can be completely tracked in real time, – enabling the connections between topology, structural stability, dynamics and function to be directly unravelled. Recent studies on nanoscale viral assemblies which found that *"concepts borrowed from macroscopic materials science are surprisingly relevant"* [48] highlight further common ground and potential synergies in concepts and techniques for unraveling self-organization across a vast range of length scales in complex materials.

Materials and Methods

Experimental apparatus and procedure.

The experiments involve an assembly of 1568 bidisperse, photoelastic disks (particles), confined in a biaxial apparatus: $\sim 80\%$ have diameter 0.74cm, $\sim 20\%$ have diameter 0.86cm. The particles rest on a flat, smooth horizontal surface, and the walls of the biax move to create specific strains, here pure shear: compression in one direction, dilation in the other, with fixed system area/density. Photoelastic materials used here are birefringent under strain. The image of a photoelastic particle, placed between crossed polarizers, shows light and dark bands that are determined by the stresses within the disk (Fig. 1 **top left**). These stresses are in turn, fixed by the (vector) contact forces acting on the particle (see Fig. 2 **left**). We solve the inverse problem for each photoelastic disk image to obtain these contact forces [16, 45]. Separate images measure the displacements, rotations and contact topology of each particle as the sample is deformed. Using this information, we can calculate the structural stability for each particle conformation [20].

The initial state is specified by: square system boundaries, a (fixed) packing fraction of $\phi = 0.795$, and as nearly isotropic and stress-free conditions as possible. We then shear the system cyclically, first by compressing/expanding in the vertical/horizontal directions, keeping the area fixed. After reaching a maximum shear deformation, we reverse the shear strain, so that there is compression/expansion along the horizontal/vertical axes. We carry out reverse shear past the configuration of square boundaries, until the shear strain reaches a minimum negative value. We again reverse the shear strain, and we return the boundaries to a square. This completes one shear cycle. Starting from the final state of the first shear cycle, we then apply similar cyclic strains for a total of six shear cycles. Each step in this process consists of a small quasi-static increment of strain (0.3%), and after each small step, we freeze the boundaries and acquire three images: one with polarizers, one without polarizers, and a third that allows us to characterize disk rotation. In the present discussion, we only examine the data for the first two shear cycles.

Structural stabilities of cluster conformations. Frictional particles in a cluster interact at their contacts through: (i) an elastic normal force given by Hooke's law (spring), (ii) an elastic-plastic tangential force given by Hooke's law if elastic and Coulomb's friction law if plastic (spring-slider combination), and (iii) an elastic-plastic contact moment analogous in form to the tangential force [20]. At each equilibrium state, we compute the stability of each cluster conformation, λ, by considering these forces using structural mechanics techniques [51, 52]. A contact through which elastic forces and moment act is termed 'elastic'; otherwise it is 'plastic'. It was proven [20] that two conservative systems S_+ and S_-, having only elastic contacts, can be constructed for any nonconservative (frictional) granular cluster so that their stabilities provide upper and lower bounds on the cluster stability. S_+ is constructed by replacing every plastic contact in the cluster with a resistive spring of stiffness equal to that used for the elastic contacts in the cluster: λ^+, the stability of S_+, bounds λ from above. S_- is constructed by replacing every plastic contact in the cluster with a spring of stiffness equal to zero, hence removing any resistance at that contact: λ^-, the stability of S_-, bounds λ from below. Stiffness matrices M_+ and M_- are then formulated for S_+ and S_- by relating the small incremental displacements du to the applied incremental loads dq as follows, $dq = Kdu$, where the matrix K ($= M_+$ or M_-) is independent of du, and is not necessarily symmetric [51, 52]. The minimum eigenvalues of M_+ and M_- are equal to the stabilities λ^+ and λ^-, respectively. The stability of the cluster conformation is expressed as $\lambda = \gamma\lambda^- + (1-\gamma)\lambda^+$ where γ is the number of plastic contacts to total number of contacts in the cluster [20]. λ has a dimensional unit of force per unit length, here N/m. Although the matrices M_+ and M_- apply to the conservative systems, they each contain information on the frictional granular cluster: i.e. the number of contacts and their individual type, position and orientation, the material properties (i.e. spring stiffness and coefficient of friction), and the boundary/loading conditions. These are all directly measurable quantities in the experiment [16, 45].

Markov transition matrix analysis. A Markov transition matrix, P, is constructed by counting the observed transitions that each cluster conformation undergoes over time steps throughout experimental loading. The states of the transition matrix are either (i) the granular cluster conformation or (ii) the interval of stability in which a granular cluster's stability property sits. The matrix P is normalized to be a row stochastic matrix and the entries of the leading left eigenvector give an approximation to the invariant density of the assumed underlying stochastic process modeling the dynamics. The approximate invariant density and P can be used to construct a time-reversible Markov matrix R whose eigenspectrum, starting with the second largest eigenvalue, can be used to determine almost-invariant transition sets [44]. Gaps in the spectrum of real eigenvalues of P indicate how many eigenvectors of R to use in order to find a given number of almost-invariant transition sets. The eigenvalue separation can also be used to gauge whether the time step interval length is appropriate. A clustering algorithm is employed to determine the (transition state) membership of each almost-invariant set by minimizing a weighted cost function, where the weighting is closely related to the approximate invariant density of each state [44].

1. Duran, J. (2000) Sands, powders, and grains: an introduction to the physics of granular media. Springer-Verlag.

2. Heinrich, M.J., Shinbrot, T., Umbanhowar, P.B. (2000) Does the granular matter? Proc. Natl. Acad. Sci. 97:12959–12960.

3. Zhu, H. P., Zhou, Z. Y., Yang, R. Y., Yu, A. B. (2007) Discrete particle simulation of particulate systems: theoretical developments. Chem. Eng. Sci. 62:3378–3396.

4. Kolymbas, D., Viggiani, G. (Eds.) (2009) Mechanics of Natural Solids Springer-Verlag.

5. Chang, C. S. (1993) Micromechanical modeling of deformation and failure for granulates with frictional contacts. Mech. Mater. 16:13–24.

6. Valanis, K. (1996) A gradient theory of internal variables. Acta Mech. 116:1–14.

7. Kolymbas, D. (2000) The misery of constitutive modelling in Constitutive Modelling of Granular Materials (ed. Kolymbas, D) 11–24.

8. Delannay, R., Louge, M., Richard, P., Taberlet, N., Valance, A. (2005) Towards a theoretical picture of dense granular flows down inclines. Nature 473:871–874.

9. Jop, Y. F., Pouliquen, O. (2006) A constitutive law for dense granular flows. Nature 441:727.

10. Tordesillas, A., Muthuswamy, M. (2008) A thermomicromechanical approach to multiscale continuum modeling of dense granular materials. Acta Geotech. 3:225–240.

11. Oda, M., Kazama, H. (1998) Microstructure of shear bands and its relation to the mechanisms of dilatancy and failure of dense granular soils. Gotechnique 48:465–481.
12. Majmudar, T. S., Behringer, R. P., (2005) Contact force measurements and stress-induced anisotropy in granular materials. Nature 435:1079–1082.
13. Rechenmacher, A. L. (2006) Grain-scale processes governing shear band initiation and evolution in sands. J. Mech. Phys. Solids 54:22–45.
14. Tordesillas, A. (2007) Force chain buckling, unjamming transitions and shear banding in dense granular assemblies, Philos. Mag. 87:4987–5016.
15. Tordesillas, A., Zhang, J., Behringer, R. P. (2009) Buckling force chains in dense granular assemblies: physical and numerical experiments. Geomech. Geoeng. 4:3–16.
16. Zhang, J., Majmudar, T. S., Tordesillas, A., Behringer, R. P. (2010) Statistical Properties of a 2D Granular Materials Subjected to Cyclic Shear, Granul. Matter 12:159–172.
17. Hall, S.A., Muir Wood, D., Ibraim, E., Viggiani, G. (2009) Localised deformation patterning in 2D granular materials revealed by digital image correlation. Granul. Matter 12:1–14.
18. Ord, A., Hobbs, B. E. (2010) Fracture pattern formation in frictional, cohesive, granular material. Phil. Trans. R. Soc. A 368:95–118.
19. Tordesillas, A., Walker, D. M., Lin, Q. (2010) Force cycles and force chains. Phys. Rev. E 81:011302.
20. Tordesillas, A., Lin, Q., Zhang, J., Behringer, R. P., Shi, J. (2011) Structural stability and jamming of self-organized cluster conformations in dense granular materials. J. Mech. Phys. Solids, 59:265–296.
21. Tordesillas, A., Walker, D. M. (2011) Deciphering D'Alemberts dream: new tools for uncovering rules for self-organized pattern formation in geomaterials. Proceedings of IWBDG11, accepted for publication.
22. Arevalo, R., Zuriguel, I., Maza, D. (2010) Topology of the force network in the jamming transition of an isotropically compressed granular packing, Phys. Rev. E 81:041302.
23. Kruyt, N.P., Antony, S. J. (2007) Force, relative-displacement, and work networks in granular materials subjected to quasistatic deformation, Phys. Rev. E 75:051308.
24. Alonso-Marroquin, F., Vardoulakis, I., Herrmann, H. J., Weatherley, D., Mora, P. (2006) Effect of rolling on dissipation in fault gouges. Phys. Rev. E 74:031306.
25. Johnson, P. A., Jia, X. (2007) Nonlinear dynamics, granular media and dynamic earthquake triggering Nat. Mater. 6:99–108.
26. Daniels, K. E., Hayman, N. W. (2008) Force chains in seismogenic faults visualized with photoelastic granular shear experiments. J. Geophys. Res. 113:B11411.
27. Perez, I., Gallego, J. (2010) Rutting prediction of a granular material for base layers of low-traffic roads. Constr. Build. Mater. 24:340–345.
28. Vivanco, F., Melo, F., Fuentes, C. (2009) Granular flow models and dilation front propagation applied to underground mining. Int. J. Bifurcat. Chaos 19:3533–3539.
29. Lemaitre, A. (2002) Rearrangements and dilatancy for sheared dense materials. Phys. Rev. Lett. 89:19.
30. Antony, S. J. (2007) Link between single-particle properties and macroscopic properties in particulate assemblies: role of structures within structures. Phil. Trans. R. Soc. A 365:2879.
31. Tordesillas, A., Muthuswamy, M., Walsh, S. D. C. (2008) Mesoscale measures of non-affine deformation in dense granular assemblies. J. Eng. Mech.-ASCE 134:1095–1113.
32. Utter, B., Behringer, R. P. (2008) Experimental measures of affine and nonaffine deformation in granular shear. Phys. Rev. Lett. 100:208302.
33. Cundall, P. A., Strack, O. D. L. (1979) A discrete numerical model for granular assemblies. Gotechnique 29:47–65.
34. Radjai, F., Wolf, D.E., Jean, M., Moreau, J.J. (1998) Bimodal character of stress transmission in granular packings. Phys. Rev. Let. 80:61–64.
35. Hartley, R. R., Behringer, R. P. (2003) Logarithmic rate dependence of force networks in sheared granular materials. Letters to Nature 421:928–931.
36. Ostojic, S., Somfai, E., Nienhuis, B. (2006) Scale invariance and universality of force networks in static granular matter. Nature 439:828–830.
37. Kruyt, N. P., Rothenburg, L. (2006) Shear strength, dilatancy, energy and dissipation in quasi-static deformation of granular materials. J. Stat. Mech.-Theory E. P07021.
38. Tordesillas, A., Muthuswamy, M. (2009) On the modelling of confined buckling of force chains. J. Mech. Phys. Solids 57:706–727.
39. Mueth, D. M. et al (2000) Signatures of granular microstructure in dense shear flows Nature 406:385–389.
40. Muhlhaus, H. B., Vardoulakis, I. (1987) The thickness of shear bands in granular materials. Gotechnique 37:271–283.
41. Schall, P., van Hecke, M. (2010) Shear bands in matter with granularity. Annu. Rev. Fluid Mech. 42:67–88.
42. Walker, D. M., Tordesillas, A. (2010) Topological evolution in dense granular materials: A complex networks perspective. Int. J. Solids Struct. 47:624–639.
43. Strogatz, S. H. (2001) Exploring complex networks. Nature 410:268–276.
44. Froyland, G. (2005) Statistically optimal almost-invariant sets. Physica D 200:205–219.
45. Zhang, J., Farhadi, R. J., Behringer, R. P., Majmudar, T. S., Tordesillas, A. (2009) A dense 2D granular material subject to cyclic pure shear. Powders & Grains AIP Conference Proceedings 1145:553–556.
46. Henzler-Wildman, K., Kern, D. (2007) Dynamic personalities of proteins. Nature 450:964–972.
47. Janssens, R.V.F. (2005) Elusive magic numbers. Nature 435:897–898.
48. Roos, W.H., Bruinsma, R., Wuite, G. J. L. (2010) Physical virology Nature Physics 6:733–743.
49. Rothenburg, L., Kruyt, N. P. (2004) Critical state and evolution of coordination number in simulated granular materials. Int. J. Solids Struct. 41:5763–5774.
50. Howell, D., Behringer, R. P., Veje, C. (1999) Stress fluctuations in a 2D granular Couette experiment: a continuous transition Phys. Rev. Lett. 82:5241–5244.
51. Bažant, Z.P., Cedolin, L. (1991) Stability of Structures: Elastic, Inelastic, Fracture and Damage Theories Oxford University Press, New York.
52. Bagi, K. (2007) On the concept of jammed configurations from a structural mechanics perspective. Granular Matter 9:109–134.

Table 1. Dominant cluster (DC) within stability bands and relationship to particles in force chains and buckled force chains. In bands 5 and 6, multiple clusters whose populations are on a par with each other dominate

Stability band	Dominant cluster	% of DC in force chain	% of buckled force chain with DC
1	2_0^0	40%	68%
2	2_0^0	43%	42%
3	3_0^0	65%	83%
4	3_0^0	65%	54%
5	$4_0^0, 4_0^1$	79%, 73%	54%, 37%
6	$4_0^0, 4_0^1, 5_0^1$	80%, 76%, 87%	31%, 16%, 18%

Fig. 1. Granular cluster conformations. Image of the assembly of photoelastic birefringent circular disks showing the force chains when sample is compressed vertically (*top left*). Subgraphs of the 28 conformations found for the experimental system throughout loading history (*top right*). Densities of conformations shown as solid line, and the most prevalent clusters classified into four almost-invariant sets distinguished by colour and symbol (*bottom left*). Representative members of three of these sets are drawn as clusters showing typical rearrangements are due to a single contact forming or breaking for the same number of disks or a new disk joins the cluster. (*bottom right*).

Fig. 2. Cooperative evolution of functional groups. Evolution of a force chain and its surrounding contacts from experiment from initial (*left*) through to final collapsed state (*right*). Conformations of member force chain particles at initial state are shown. As buckling commences, 3-cycles prop-up the buckling chain to restore alignment: e.g. note the increasing birefringence brightness from the left (right) 3-cycle supporting the 2nd-3rd (1st, 5th-6th) particles from the bottom of the chain before collapse.
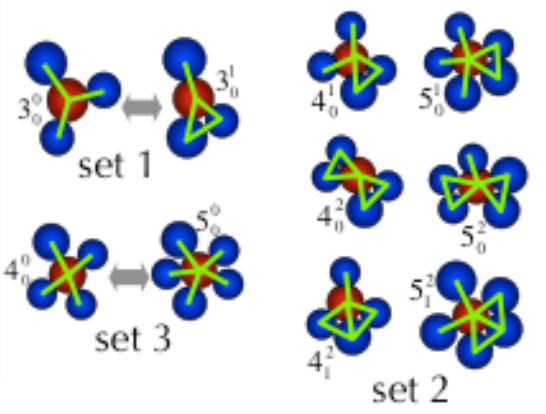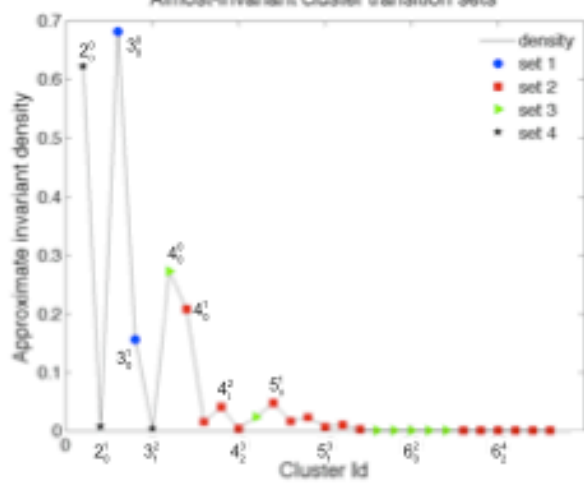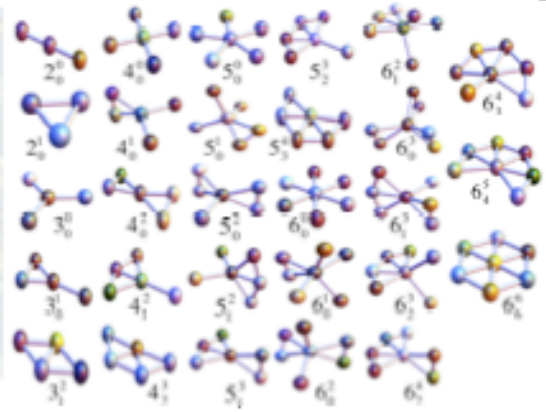
Fig. 3. Stability landscape. The landscape of stability during loading showing the most prevalent granular conformations found in the most resolved stability bands of the cyclic shear experiment.

Fig. 4. Favoured pathways and dynamical barriers in the stability landscape. Scaled entries of the Markov transition matrix reveal the block structure of the stability bands (*left*). The approximate invariant density of the stability transition matrix revealing the preferred stability peaks (*top right*). Sudden changes in the entries of the second largest eigenvector correspond to the transition matrix blocks and determine the stability band barriers indicated by alternating solid and dashed lines (*bottom right*).

Fig. 5. Force chains need lateral support for stability. Cumulative distribution function (CDF) of stability of force chain particle conformations (red square) and non-force chain conformations (blue triangle). Force chain particle conformations generally possess higher stability. (*Inset*) The six stability band transition probabilities of buckled force chain (BFC) particle clusters are typically within the same band (diagonally dominant) or to a lower stability band; probabilities below the diagonal are greater than those above the diagonal.
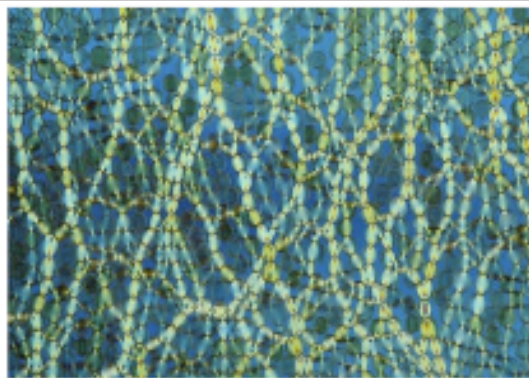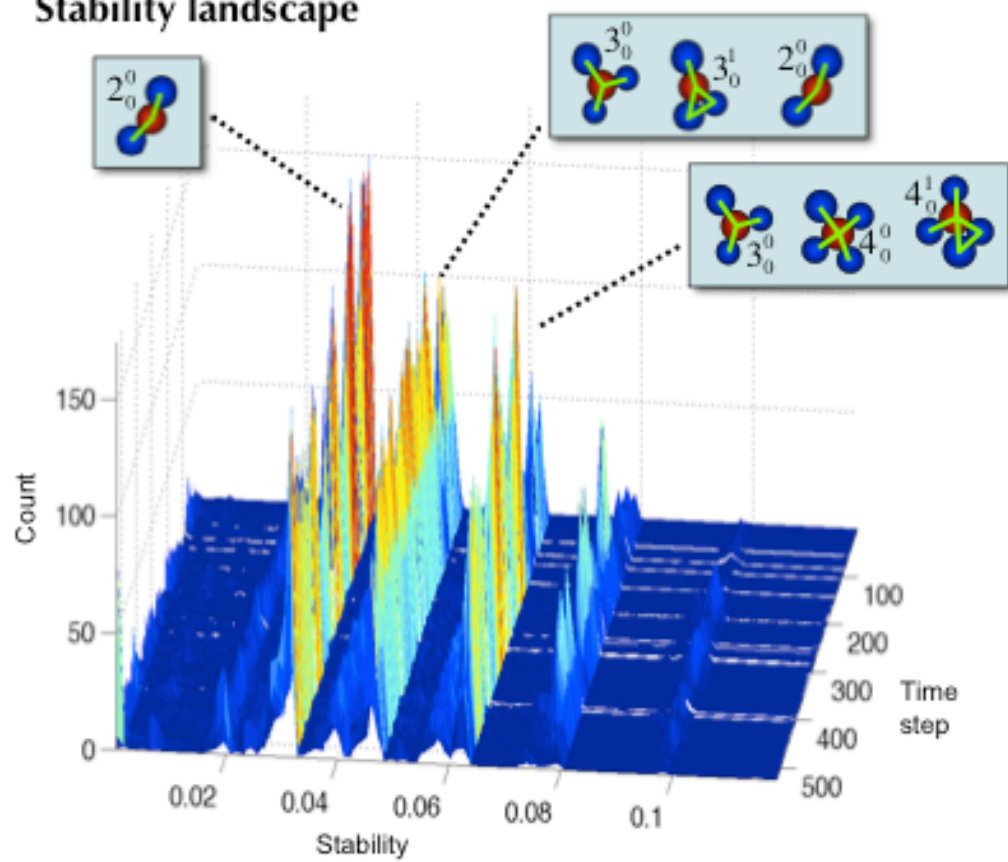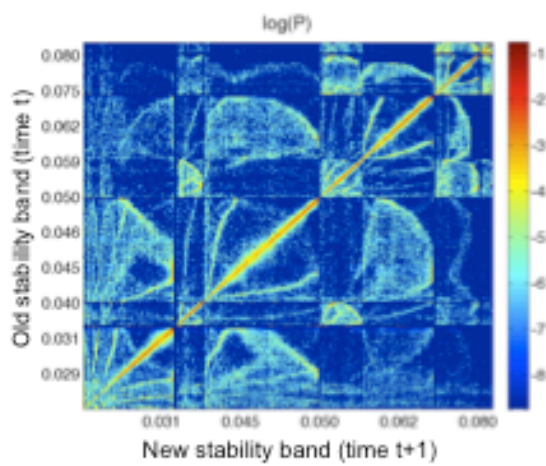
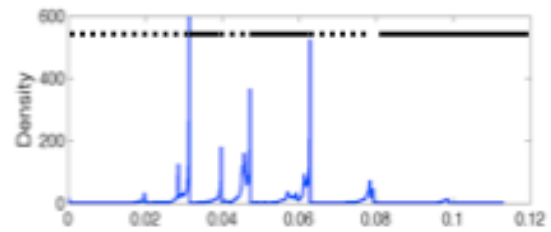Almost-invariant cluster transition sets
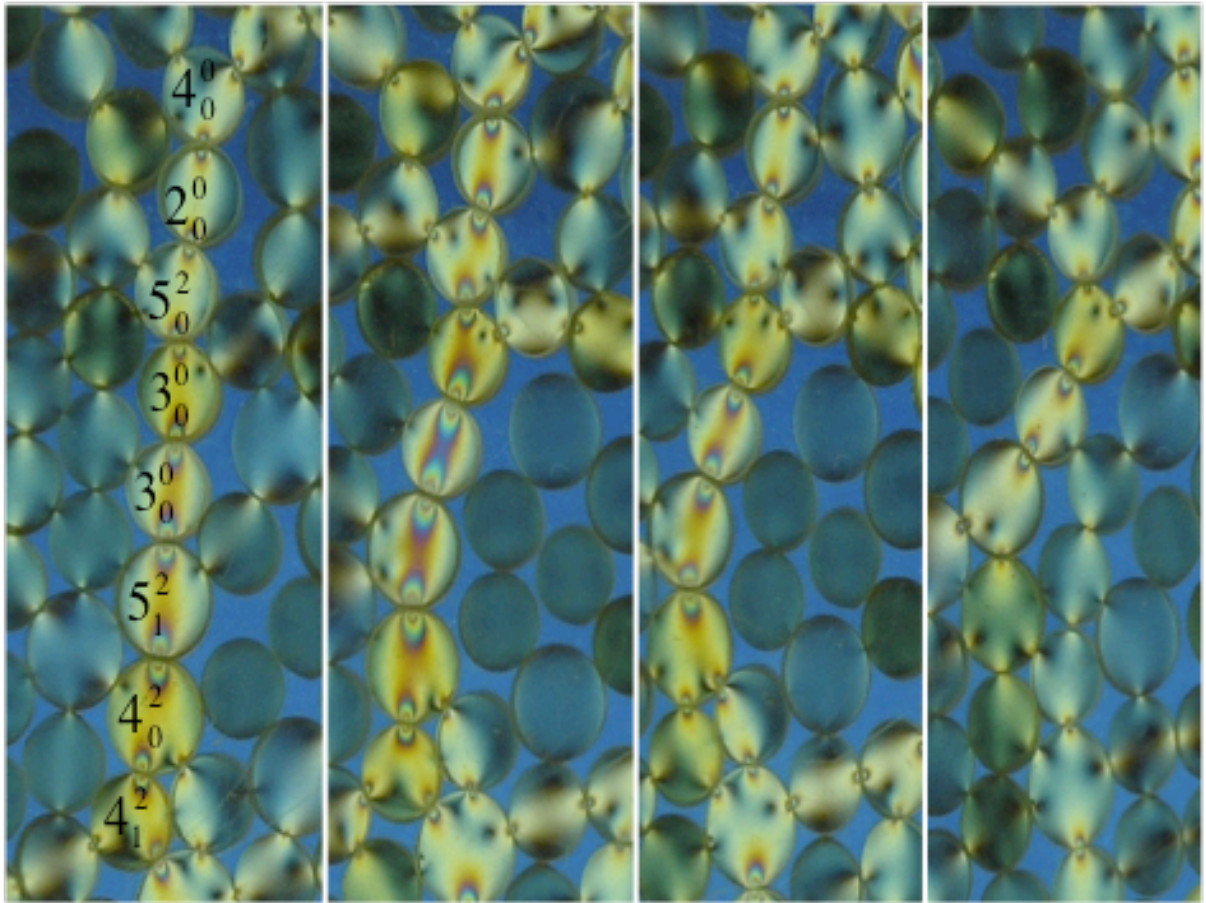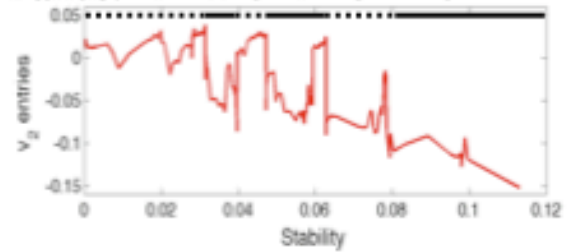
Stability landscape

Transition matrix

log(P)

Old stability band (time t)

New stability band (time t+1)

**Spectral properties
(Aggregated stability bands)**

Bands: 1 2 3 4 5 6

Density

Bands: 1 2 3 4 5 6

V_2 entries

Stability

Conformational stability

BFC stability transitions